JOURNAL OF THERMOPHYSICS AND HEAT TRANSFER
Vol. 8, No. 4, Oct.–Dec. 1994

Flow Resolution and Domain Influence in Rarefied Hypersonic Blunt-Body Flows

Brian L. Haas*
NASA Ames Research Center, Moffett Field, California 94035
and
Michael A. Fallavollita†
Stanford University, Stanford, California 94305

This parametric study assesses the influence of upstream domain size and grid resolution upon flowfield properties and body aerodynamics computed for rarefied flows over cold blunt bodies with a direct simulation Monte Carlo (DSMC) particle method. Empirical correlations are suggested for aerodynamic coefficients for two-dimensional flows past a perpendicular flat plate. Freestream parameters that were varied in the study include the Mach number, Knudsen number, surface temperature, and intermolecular potential. Insufficient grid resolution leads to overprediction of aerodynamic heating and forces in the DSMC method. Molecular diffusion from the body surface results in greater far-field domain influence as flow rarefaction increases. As a result, insufficient upstream domain size in the DSMC method leads to overprediction of heating and drag. Simulation of a hard sphere gas is more sensitive to grid resolution, whereas simulation of a Maxwell gas is more sensitive to upstream domain size. Finally, a simple study of normal shock waves indicates that a grid cell dimension less than one-third of the upstream mean free path is required to capture shock profiles accurately.

Nomenclature

C = aerodynamic force coefficient
H = plate height
Kn = Knudsen number, λ/H
$\overline{Kn}$ = Whitfield's correlation parameter, Eq. (6)
L = upstream domain size
$\bar{L}$ = domain size correlation parameter, Eq. (16)
M = Mach number
Nu_w = Nusselt number at the wall, Eq. (7)
n = gas number density
Pr = Prandtl number, Eq. (8)
Q = freestream kinetic heat flux, $\rho_\infty u_\infty^3/2$
q = aerodynamic net heat flux
Re = Reynolds number, Eqs. (2) and (3)
St = Stanton number, Eq. (9)
T = temperature
u = flow velocity
x = location relative to stagnation point
$\bar{x}$ = distance from plate to T half-rise location
α = intermolecular potential exponent
γ = ratio of specific heats, 1.4
δ = length of a cubic grid cell
λ = gas mean free path
ρ = gas mass density

Subscripts
a = adiabatic wall condition
D = drag
ERR = error coefficient
L = lift over top half of body
r = pertains to rotational mode
s = stagnation value
t = pertains to translational mode
w = wall value
∞ = freestream value

Superscripts
DOM = pertains to domain effects
RES = pertains to resolution effects
$*$ = presumed-correct value

Received Oct. 25, 1993; revision received March 14, 1994; accepted for publication March 25, 1994. Copyright © 1994 by the American Institute of Aeronautics and Astronautics, Inc. No copyright is asserted in the United States under Title 17, U.S. Code. The U.S. Government has a royalty-free license to exercise all rights under the copyright claimed herein for Governmental purposes. All other rights are reserved by the copyright owner.

*Research Scientist, Thermosciences Institute. Member AIAA.
†Research Assistant, Department of Aeronautics and Astronautics. Student Member AIAA.

Introduction

FLOWFIELD characteristics about blunt bodies during atmospheric entry lead to considerable challenges for computational simulation. Highly rarefied flows, where the gas density n is low and the mean free path λ between molecular collisions is high, are better suited to particle simulation methods, such as the direct simulation Monte Carlo (DSMC) technique pioneered by Bird,[1] rather than continuum techniques based upon the Navier-Stokes equations. DSMC methods employ many model particles whose motion and interaction simulate gas dynamics directly. The simulated flowfield is divided into a network of small cells to facilitate collision modeling and statistical sampling.

The computational burden of DSMC methods, however, grows proportionally with local gas density and the size of the computational domain. In typical entry flows, the body surface temperature is rather low compared with the stagnation temperature, leading to a steep density gradient near the body surface. Accurate simulation of this flowfield requires sufficient grid resolution near the body. Alternatively, the extent of freestream rarefaction results in a leading shock layer that is fully merged with the boundary layer of the body, yet extends far upstream. Accurate simulation therefore requires a large upstream computational flow domain. Together, these requirements rapidly drive the computational cost of the particle simulation method upward. Hermina[2] and Woronowicz[3] studied grid resolution effects for flows over slender bodies and flat plates parallel to the freestream direction. In contrast, the present study addresses flow over blunt bodies. Also, errors resulting from limited domain size became evident in

recent computations of aerobraking of the Magellan spacecraft.[4] The DSMC researcher must therefore understand what simulation costs are necessary to obtain a solution of sufficient accuracy.

The objective of the present parametric study was to assess quantitatively the sensitivity of aerodynamic loads and gas properties to grid resolution and simulation domain size in blunt-body, hypersonic, rarefied flows. These results allow the researcher to make an intelligent tradeoff between simulation cost and accuracy. In addition, correlations are suggested for aerodynamic coefficients and flowfield properties over a wide range of freestream conditions.

Methods of Analysis

The present study employed an efficient particle simulation technique[5,6] to investigate the net heat flux q and aerodynamic forces on a two-dimensional flat plate of height H facing perpendicular to the flow direction. Gas temperature T and number density n were also computed along the stagnation streamline. The following ranges of flow conditions were used:

$$M_\infty = \{5, 10, 20\}$$
$$Kn_\infty = \{0.1, 0.3, 1, 3, 10\}$$
$$T_w/T_\infty = \{1, 5, 9\}$$
$$\alpha = \{4, 8, \infty\}$$

For each flow case, the gas was modeled with two fixed internal DOF leading to a constant ratio of specific heats of $\gamma = 1.4$. Interaction of the gas with the plate surface at wall temperature T_w was modeled as fully diffuse and thermally accommodated. All simulations employed between 4–64 particles per cell as the input freestream number density n_∞. The code used cubic Cartesian cells of uniform dimension throughout the flowfield, but this does not alter the conclusions of the present work when applied to DSMC codes with variable cell dimensions.

For each set of flow conditions, the simulation resolution and domain were varied considerably and their effects upon solution accuracy were determined. Grid resolution is defined by H, whereas the flowfield domain size is defined by the distance L of the computational field upstream of the plate, where both H and L are measured in units of grid cells of linear dimension δ. These length scales are depicted schematically in Fig. 1 along with $\bar{x}$ that represents the location, far upstream of the plate, where the local translational temperature first reaches half of its peak value.

To estimate the local mean free path length in the DSMC technique, note that any two particles in the flow may collide with one another only if they both reside in the same grid cell. Furthermore, any two particles within a given cell can collide with one another regardless of their respective positions in the cell. The collision probability for a particular pair of neighboring particles is assessed as a function of molecular constants and the relative translational energy of the pair.[5] If the cell dimension δ near the cold body surface is too large, then energetic particles at the far edge of the cell are able to readily transmit momentum and energy to particles immediately adjacent to the surface. The latter particles may, in turn, transmit that energy and momentum to the surface. This leads to overprediction of both the surface heat flux and the aerodynamic force on the body than would occur in the real gas. This error is minimized by reducing the cell dimension relative to the local mean free path of molecules near the surface. From equilibrium kinetic theory, where translational velocities have a Maxwellian distribution, the local λ is related to the local n and T as follows:

$$(\lambda/\lambda_\infty) = (n_\infty/n)(T/T_\infty)^{2/\alpha} \quad (1)$$

The exponent of the assumed inverse-power intermolecular potential α may vary between the limits of the Maxwell molecule ($\alpha = 4$) and the hard sphere ($\alpha = \infty$). The expression in Eq. (1) is not exact for flows far from translational equilibrium, but will suffice to characterize the degree of rarefaction in the flow. Employing the stagnation temperature and density near the plate surface from the DSMC simulation leads to an approximation of the stagnation mean free path λ_s. Theoretical estimates of λ_s were derived by Whitfield,[7] but were limited to particular flow conditions and were not as convenient as the simple expression in Eq. (1) for use in the present study.

As a consequence of Eq. (1), regions of high density lead to short mean free paths, requiring finer cell resolution to capture flowfield gradients accurately. Such behavior characterizes hypersonic rarefied flows near cold blunt-body surfaces.

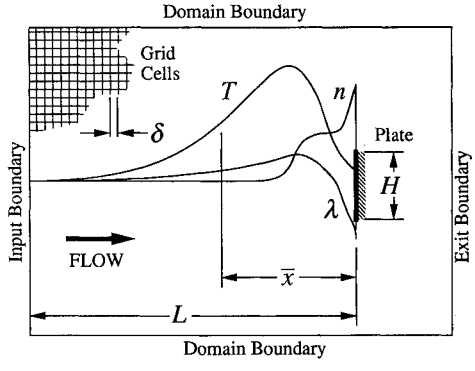

Fig. 1 Definition of simulation length-scales and schematic representation of temperature and density profiles upstream of a cold plate of dimension H in rarefied flow.

Flowfield Characteristics and Correlations

Having computed flowfield properties and aerodynamics over a wide range of input conditions and simulation parameters, it proved instructive to summarize the most accurate results, i.e., those corresponding to grids of sufficient resolution and domains of sufficient size.

Flow Along the Stagnation Streamline

Density profiles along the stagnation streamline upstream of the plate are plotted in Fig. 2a to demonstrate the effects of freestream rarefaction. Note that the density at the plate surface (at $x/H = 0$) is significantly higher than the freestream value. This behavior is slightly more pronounced, and the gradients are steeper, for flows at lower Kn_∞. This, combined with the fact that lower Kn_∞ means that the freestream λ_∞ is short, dictates that the cell resolution must be very fine compared with more rarefied flows. Notice that there is no real shock structure ahead of the body except at the lowest Kn_∞.

Temperature profiles along the stagnation streamline for these same flows are plotted in Fig. 2b. Temperature was defined by the variance of particle velocities. These curves clearly demonstrate that the body influences the flowfield far upstream. This domain of influence increases with Kn_∞ as a result of upstream diffusion of particles that reflected from the body surface. By contrast, Kn_∞ has little effect upon the resultant stagnation temperature and density at the plate surface.

For a given freestream Knudsen number, the effects of Mach number on the streamline profiles are demonstrated in Fig. 3. Greater Mach number leads to significantly greater stagnation density and temperature, as well as greater peak temperature. However, unlike Kn_∞, M_∞ has very little effect on the extent of the domain of influence upstream of the plate.

As is evident in the profiles in Fig. 4, however, T_w affects all flowfield properties including the peak temperatures, stagnation values, and the extent of the domain of influence of the plate in these rarefied flows. This results from particles

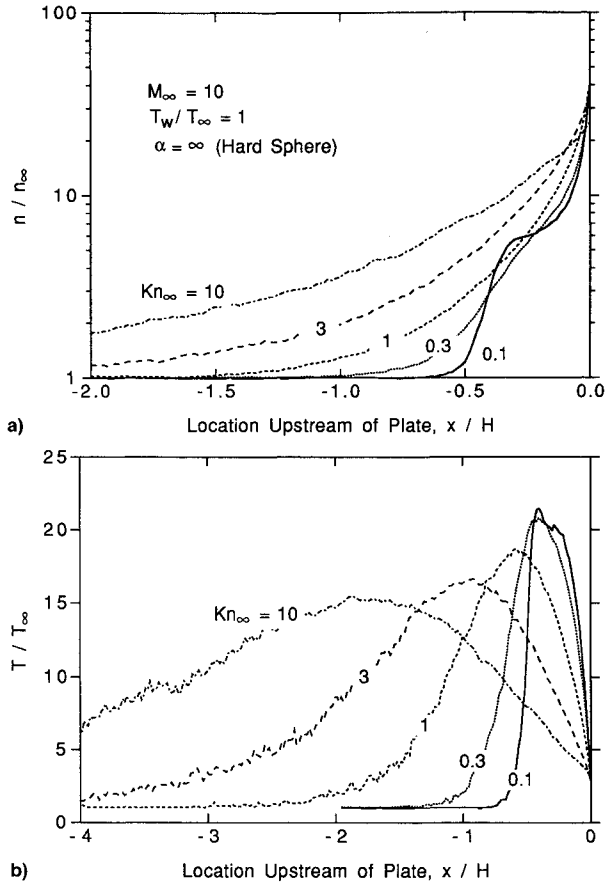

Fig. 2 Effects of flow rarefaction Kn_∞ upon profiles along the stagnation streamline: a) number density and b) temperature.

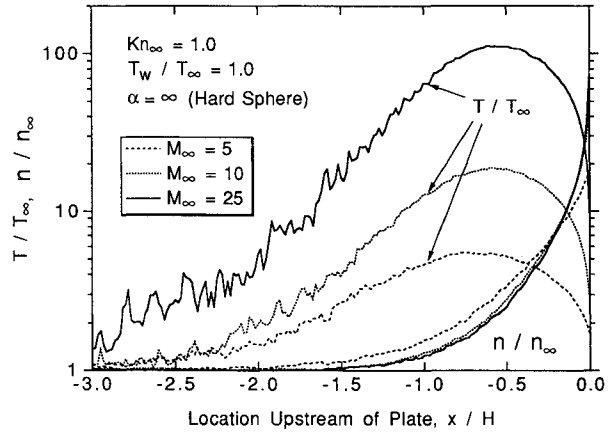

Fig. 3 Effects of Mach number upon profiles along the stagnation streamline.

reflecting from hotter surfaces with greater energies, leading to greater relative translational velocities and flowfield temperatures. Energetic reflections from the hotter surface reduce the net buildup of particle density near the plate.

Finally, the effects of employing different exponents α of the intermolecular potential are demonstrated in Fig. 5. Just as with Kn_∞, different potentials have little effect upon the stagnation temperature or density, but lower values of α greatly increase the extent of the domain of influence upstream of the body. Plotting the local mean free path as computed with Eq. (1) shows that λ is much greater for $\alpha = 4$ than for $\alpha = \infty$. The flow therefore becomes effectively more rarefied, and the profiles are indicative of those corresponding to large Kn_∞ in Fig. 2. Also, the gradients for the hard sphere are steeper and lead to lower λ_s at the stagnation point on the body compared to the Maxwell molecule. These observations are

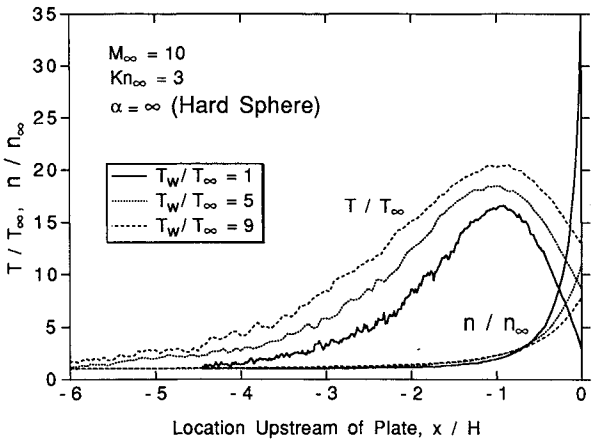

Fig. 4 Effects of wall temperature upon profiles along the stagnation streamline.

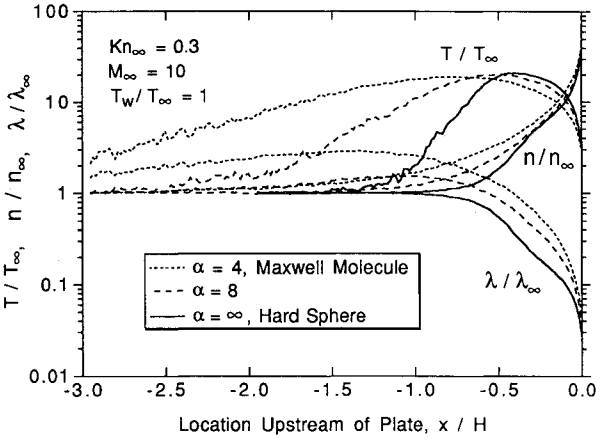

Fig. 5 Effects of intermolecular potential upon profiles along the stagnation streamline.

consistent with the interpretation that the Maxwell molecule has a more viscous, diffusive nature than the hard sphere molecule because of its greater cross section. As a consequence, accurate DSMC solutions for hard sphere gases require finer cell resolution, whereas solutions for Maxwell molecule gases require larger upstream computational fields.

Many of these effects are summarized by plotting λ_s and $\bar{x}$ for all flow conditions. The stagnation mean free path correlated fairly well with the product $Re_w Kn_\infty^{3/4}$ as plotted in Fig. 6. The Reynolds number based on the wall temperature is defined from the temperature dependence of the coefficient of viscosity and is given by

$$Re_w = Re_\infty (T_\infty/T_w)^{1/2 - 2/\alpha} \tag{2}$$

where the freestream Reynolds number is determined from Bird's definition of mean free path[8] as follows:

$$Re_\infty = \tfrac{2}{15}(6 - 4/\alpha)(4 - 4/\alpha)(\gamma/2\pi)^{1/2}(M_\infty/Kn_\infty) \tag{3}$$

Employing a least-squares log-log fit to the data in Fig. 6 leads to the following simple expression for the stagnation mean free path for these flows

$$\lambda_s = \lambda_\infty/(2Re_w Kn_\infty^{3/4}) \tag{4}$$

This correlation takes into account the effects of all flow parameters (M_∞, Kn_∞, α, and T_w), and demonstrates that λ_s is strongly dependent upon M_∞ and weakly upon Kn_∞.

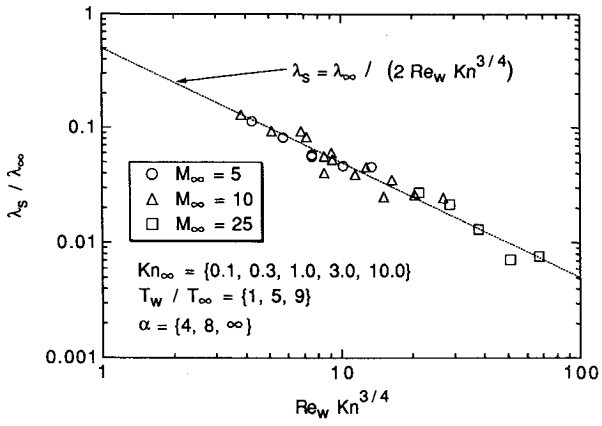

Fig. 6 Empirical correlation for the stagnation mean free path.

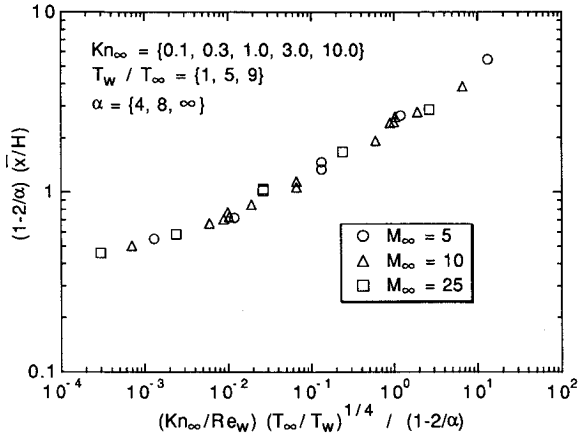

Fig. 7 Empirical correlation for the extent of the domain of influence upstream of the body.

As plotted in Fig. 7, the upstream extent $\bar{x}$ of the domain of influence of the body is correlated against the product

$$\left(\frac{1}{1 - 2/\alpha}\right)\left(\frac{T_\infty}{T_w}\right)^{1/4}\frac{Kn_\infty}{Re_w} \tag{5}$$

Again, this gives a fair correlation and encompasses all parameters. Here, $\bar{x}$ exhibits stronger dependence upon Kn_∞ than upon M_∞.

All correlations suggested in the present study were developed through parameterization. That is, simulation results for cases with identical flow conditions except for a given parameter were compared with each other to assess dependence upon the given parameter. Simulation results were plotted using quantities multiplied by powers of the independent parameters.

Correlations for Aerodynamic Coefficients

No existing theory describes completely the heating and aerodynamic loading of bodies over the entire range of Reynolds number. The objective here is only to estimate the dependencies of the aerodynamic coefficients upon flow conditions empirically, rather than develop a detailed theory for them. In addition to numerous experimental investigations, previous computational attempts to identify correlation parameters have met with some success, including those of Woronowicz[9] for flat plates parallel to the freestream flow, and Gilmore and Harvey[10] for flat-ended cylinders. The latter work concludes that $\overline{Kn}$, defined by

$$\overline{Kn} = Kn_\infty[\sqrt{\gamma(\pi/2)(T_\infty/T_w)}M_\infty + 1]^{-1} \tag{6}$$

is reasonable for correlating heat transfer. The results of the present study employed this parameter to correlate Nu_w, divided by $\sqrt{Kn_\infty}$, to obtain the result plotted in Fig. 8. Here, Nu_w is defined from the following expressions:

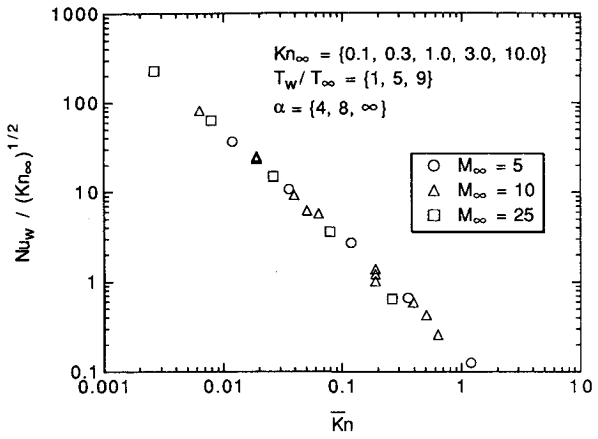

Fig. 8 Empirical correlation for plate heating.

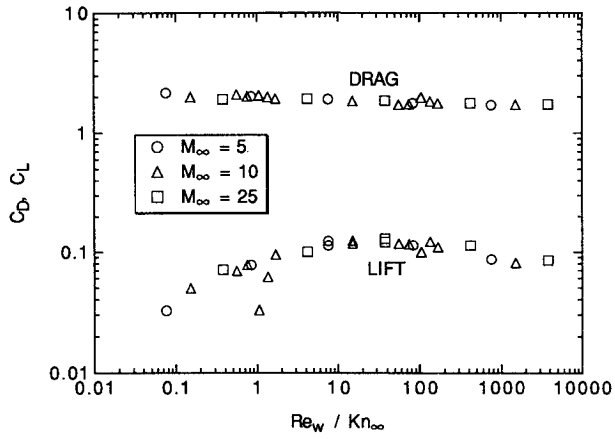

Fig. 9 Empirical correlation for plate drag and lift forces.

$$Nu_w = Re_w PrSt \tag{7}$$

$$Pr = \frac{4\gamma}{9\gamma - 5} \tag{8}$$

$$St = \frac{\gamma - 1}{2}M_\infty^2\frac{q/Q}{(T_a/T_\infty) - (T_w/T_\infty)} \tag{9}$$

$$\frac{T_a}{T_\infty} \approx 2\frac{\gamma - 1}{\gamma + 1}\left(\frac{\gamma}{\gamma - 1} + \frac{\gamma}{2}M_\infty^2\right) \tag{10}$$

The last expression closely approximates the adiabatic wall temperature for free molecule flows[11] and is assumed to be a fair estimate for the rarefied flows studied here.

Aerodynamic drag and lift on the plate did not vary significantly among the flow cases, but did exhibit some weak correlation to the ratio Re_w/Kn_∞ as plotted in Fig. 9. In the present context, the lift coefficient C_L is defined by the body force, perpendicular to the flow direction, over the top half of the plate only. Defining C_L in this way yields a parameter that will prove below to be sensitive to grid resolution and domain size. Naturally, integrating the force over the top and bottom halves of the plate would yield zero lift force due to symmetry.

Grid Resolution

For all flow conditions within the Knudsen number range, $0.1 \leq Kn_\infty \leq 1.0$, simulations were performed to assess the effects of grid resolution upon solution accuracy. Since all flow parameters and aerodynamic coefficients are normalized

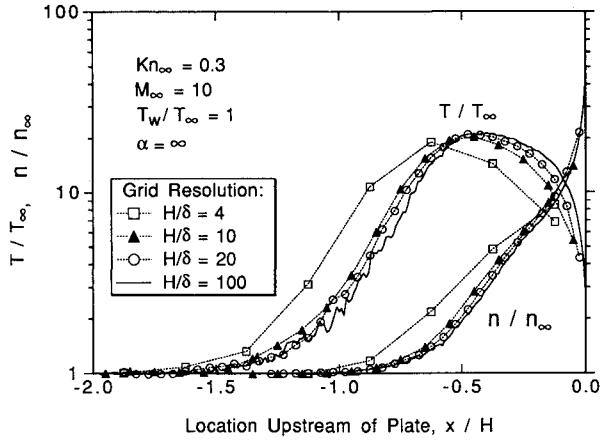

Fig. 10 Effect of grid resolution upon profiles along the stagnation streamline upstream of the plate.

by the plate height, grid resolution was defined by the ratio H/δ. At each flow condition, simulations were performed using plates measuring $H/\delta = \{2, 4, 6, 10, 20, 40, 60, 100, 200, 400\}$. Although simulation accuracy in the flow scenario described here is dominated by grid resolution at the body surface, the ability to capture shock wave profiles is also sensitive to resolution. A simple grid study was performed for the simple one-dimensional shock flow problem and the results are presented in the Appendix.

Resolution Effects on Flowfield Profiles

The density and temperature profiles along the stagnation streamline ahead of the body are plotted in Fig. 10 for $Kn_\infty = 0.3$. For the coarse grids, where $H/\delta < 100$, the profiles were smeared considerably. For $H/\delta \geq 100$, the profiles coalesced to a single form and were assumed therefore to represent accurate solutions. This same general behavior was observed for all flow conditions, although the resolution required to capture the appropriate profiles did not need to be as fine at larger Kn_∞ compared with lower Kn_∞. For example, at $Kn_\infty = 1.0$, accurate profiles were obtained at $H/\delta \geq 60$.

Resolution Effects on Aerodynamic Coefficients

For each simulation, the coefficients for heating and aerodynamic forces were computed. To assess the errors corresponding to a given flowfield resolution, the aerodynamic coefficients computed with the finest resolution at each flow condition were assumed to represent the "correct" values for that flow. It was the stagnation density and temperature from that solution that was also used to determine λ_s as plotted in Fig. 6.

As observed qualitatively for all flow conditions, coarse grid resolution led to overprediction of heating, drag, and lift. The errors dropped considerably with finer resolution. Errors in the aerodynamic coefficients were correlated and plotted against the product $\lambda_s Re_w/\delta$ in Fig. 11. Best agreement was obtained, through parameterization, by employing error coefficients defined as follows:

$$(q)_{\mathrm{ERR}}^{\mathrm{RES}} = 10^{4/\alpha}(Kn_\infty/Re_w)^{1/2}[(q/q^*) - 1] \quad (11)$$

$$(C_D)_{\mathrm{ERR}}^{\mathrm{RES}} = 5^{4/\alpha}[(C_D/C_D^*) - 1] \quad (12)$$

$$(C_L)_{\mathrm{ERR}}^{\mathrm{RES}} = Re_w^{-1/2}[(C_L/C_L^*) - 1] \quad (13)$$

Superscript * denotes the value for the coefficient that was assumed to be most accurate from the finest resolution simulation. These plots provide an engineering assessment of the accuracy associated with a given grid resolution, in terms of stagnation mean free path, for a given set of flow conditions. Scatter in the plots resulted from imperfect correlation parameters and the statistical limitations inherent to the DSMC technique. Scatter is particularly noticeable at the highest resolutions where the errors are small relative to the accuracy of the simulation method.

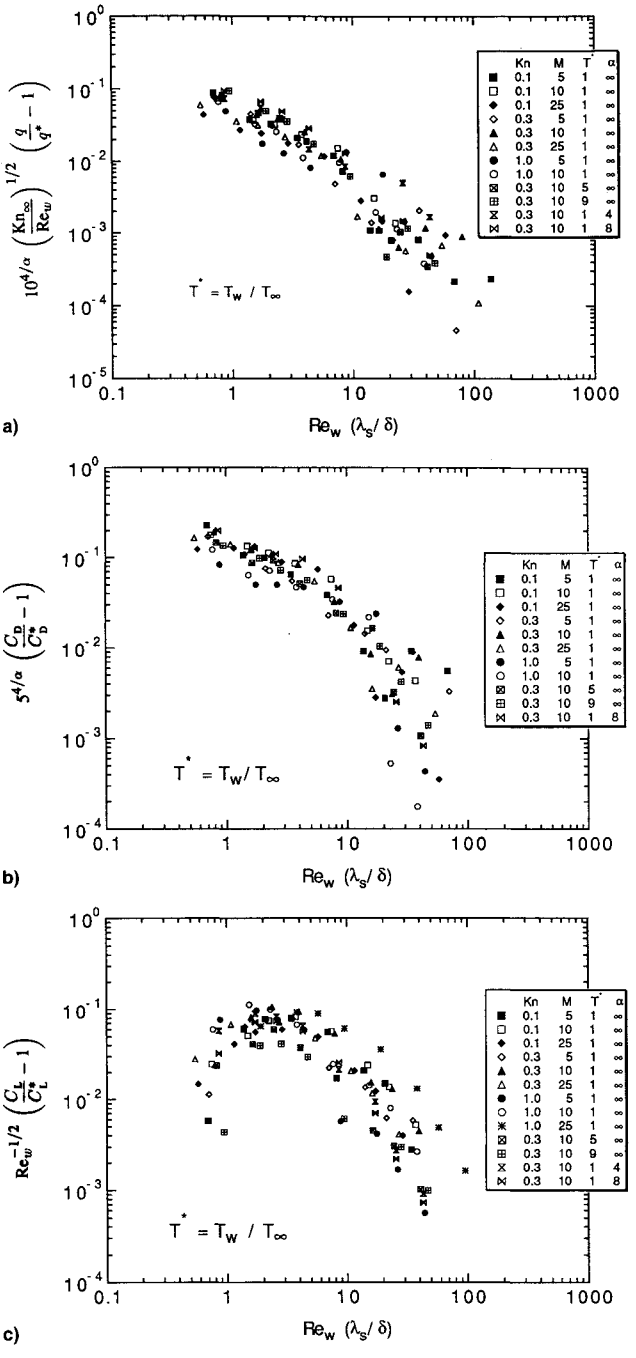

Fig. 11 Correlated effect of DSMC grid resolution upon aerodynamic coefficients for all flow conditions: a) heating, b) drag, and c) lift.

Domain Size

For rarefied flows in the higher Knudsen number range ($1.0 \leq Kn_\infty \leq 10.0$), simulations were performed to assess the influence of the upstream flowfield domain upon solution accuracy. In view of the results above, the cell resolution used in each case here was sufficiently fine such that the stagnation mean free path exceeded one cell-length near the body. The objective here was to employ different upstream computational field sizes, defined by L in Fig. 1, to determine the minimum acceptable domain size required for a given penalty in solution accuracy. At each flow condition, simulations were performed using domains of dimensions $L/H = \{0.1, 0.2, 0.5, 1, 2, 4, 8, 16, 32\}$.

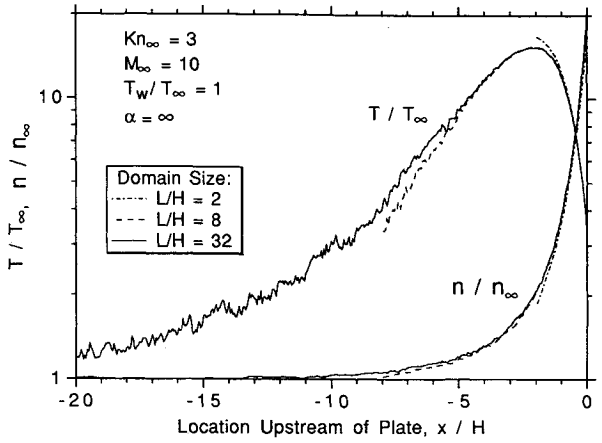

Fig. 12 Effect of DSMC domain size upon profiles along the stagnation streamline upstream of the plate.

Domain Size Effects on Flowfield Profiles

Flowfield density and temperature along the stagnation streamline are plotted for one flow condition in Fig. 12 employing different domain sizes L. With sufficiently large L, all the curves coalesced to a single curve to represent the assumed correct profile as represented at $L/H = 32$. With insufficient upstream domain (i.e., small L), density and upstream temperature are underpredicted while the peak temperature is overpredicted. However, once the simulation domain size exceeded roughly twice the distance of the temperature half-rise point $\bar{x}$, the temperature and density profiles followed the expected forms predicted when ample upstream domain was employed. Although not presented here, behavior for all other flow conditions are qualitatively similar to these results.

Domain Size Effects on Aerodynamic Coefficients

Quantitative assessment of the errors in aerodynamic loads on the plate for simulations employing different upstream domain sizes are presented in Fig. 13. The errors for each case are computed relative to the aerodynamic loads that were obtained using the largest domain L and presumably represent the correct values. Each plot employs a length scale normalized by $\bar{x}$. As expected, the errors in predicted aerodynamics decreased as larger upstream domain sizes were used. Aerodynamic heating q and drag C_D were overpredicted in all cases. The lift forces were so small for these rarefied flows that the errors for each domain size were negligible relative to the statistical fluctuation of the simulation, and were therefore not plotted. Through parameterization, the best correlations over the range of flow conditions employed error coefficients defined by

$$(q)_{\mathrm{ERR}}^{\mathrm{DOM}} = \left(\frac{1 + 4/\alpha}{1 - 2/\alpha}\right) Kn_\infty^{3/2} \left(\frac{T_\infty}{T_w}\right)^{1/8} \left(\frac{q}{q^*} - 1\right) \quad (14)$$

$$(C_D)_{\mathrm{ERR}}^{\mathrm{DOM}} = \left(\frac{1 + 4/\alpha}{1 - 2/\alpha}\right) Kn_\infty^{3/2} \left(\frac{T_\infty}{T_w}\right)^{1/8} \left(\frac{C_D}{C_D^*} - 1\right) \quad (15)$$

and a domain-size correlation-parameter given by

$$\bar{L} = (L/\bar{x})(T_\infty/T_w)^{1/8}[1/(1 + 2/\alpha)] \quad (16)$$

Note that the data levels off as the $\bar{L}$ drops below roughly 0.3. In the limit of decreasing upstream domain, the incoming flow is almost completely unaffected by particles reflecting from the plate surface such that the aerodynamic loads approach the values corresponding to the free molecular flow limit. For heating and drag, the limit is less erroneous for flows at greater Kn_∞, since free molecular flow represents the limit of greatest possible rarefaction. The interesting paradox

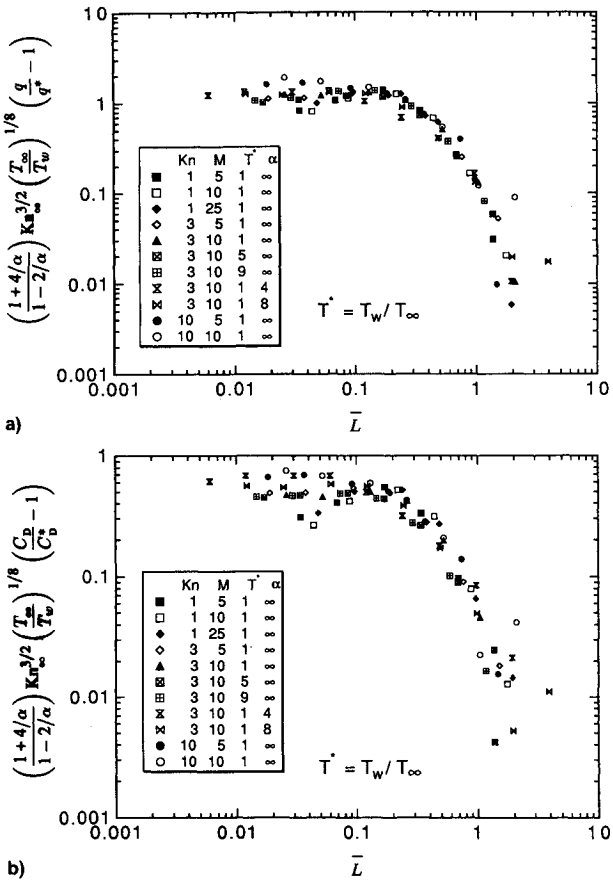

Fig. 13 Correlated effect of DSMC domain size upon aerodynamic coefficients for all flow conditions: a) heating and b) drag.

is that, while the domain of upstream influence increases with Kn_∞, the penalty in terms of solution accuracy is less dramatic compared to simulations at lower Kn_∞.

Concluding Remarks

When employing direct particle simulation methods, accurate simulation of highly rarefied flows about cold blunt bodies requires sufficient computational grid resolution and upstream flowfield domain size. The objective of this parametric study was to assess quantitatively the penalty suffered in solution accuracy when minimizing computational expense by using short domains and coarse grids. Qualitative results were similar for all freestream conditions. Empirical correlations were also suggested for stagnation streamline properties and aerodynamic loading over the range of flow conditions.

Accuracy penalties for grid resolution and domain size were expressed in terms of flowfield properties λ_s and $\bar{x}$. These results indicate that no single criterion or "rule-of-thumb" exists to specify suitable simulation parameters for all flow scenarios. Rather, the researcher must tradeoff the costs associated with a given resolution and domain size with the accuracies estimated for the particular flow simulation. This assessment may be done through the use of the plots presented in the present work. Nonetheless, as concluded in the Appendix, a simple criterion given by $\delta < \lambda_\infty/3$ may be specified for accurate simulation of normal shock wave profiles.

The quantitative results of the present work apply specifically to the two-dimensional flow about a flat plate perpendicular to the freestream direction when $\gamma = 1.4$. However, they likely apply reasonably well to any cold-wall, blunt-body, hypersonic, rarefied flow problem.

Appendix: Shock Wave Resolution Study

When specifying cell sizes throughout the flowfield, it is helpful to understand quantitatively the effects of grid reso-

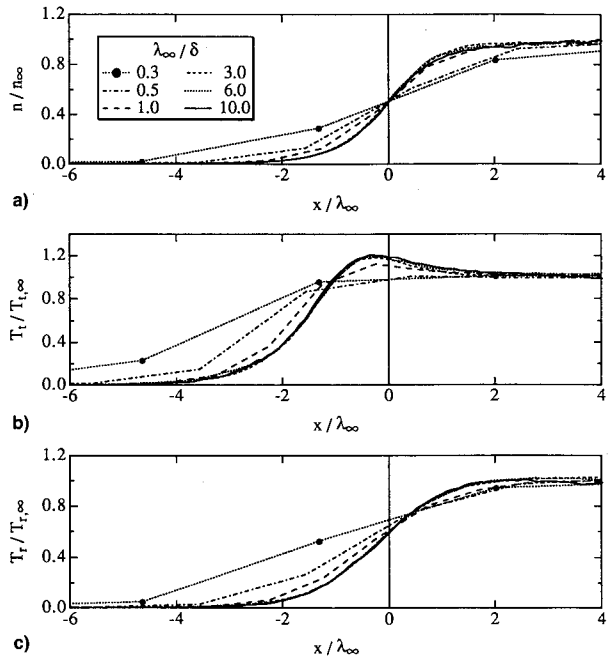

Fig. A1 Effects of grid resolution on shock wave profiles, simulated at $M_\infty = 20$ and $\gamma = 1.4$, for a) density, b) translational temperature, and c) rotational temperature.

lution on the DSMC solution. While insufficient grid resolution can reduce significantly the accuracy of predicted aerodynamic heating and forces in blunt-body flows, it can also smear density and temperature profiles in normal shock waves.

To compliment the blunt-body results above, a series of one-dimensional shock flows were simulated with the DSMC method using grids of differing resolution. A single representative flow condition was simulated pertaining to a hard sphere diatomic gas at $M_\infty = 20$ and $\gamma = 1.4$ in the freestream. Neglecting the vibrational mode, the rate of internal energy excitation was specified arbitrarily by a fixed rotational collision number of 5. The grid cells were cubic and uniform throughout the flowfield, with linear dimensions δ defined relative to the freestream λ_∞. The six simulation cases were specified respectively by $\lambda_\infty/\delta = \{0.3, 0.5, 1, 3, 6, 10\}$.

Profiles of density, translational temperature, and rotational temperature are plotted in Fig. A1. Given sufficient relaxation distance, the pre- and postshock conditions for all cases were identical, matching the expected Rankine-Hugoniot shock jump conditions. However, the shock profiles were smeared considerably for coarse resolutions given by $\lambda_\infty/\delta < 3$. With all profiles centered at a common half-rise point for density in Fig. A1a, note that the coarse temperature profiles are smeared and are further upstream of the density shock than those obtained with finer grid resolutions. Furthermore, coarse resolution fails to capture the overshoot in translational temperature associated with finite rotational relaxation in the shock. Simulations for flow at $M_\infty = 5$ yielded identical results.

Acknowledgments

This work is sponsored in part (for BLH) by NASA Cooperative Agreement NCC2-582 to Eloret Institute, and (for MAF) by NASA Grant NCA 2-693 and Air Force Office of Scientific Research Grant AFOSR 90-0232. The authors would like to thank Wahid Hermina (Sandia National Laboratories) for helpful discussions that led to this parametric study. The authors acknowledge and appreciate the support of NASA Ames Research Center and the Numerical Aerodynamic Simulation for the use of their facilities.

References

[1]Bird, G. A., *Molecular Gas Dynamics*, Clarendon Press, Oxford, England, UK, 1976.

[2]Hermina, W. L., "Monte Carlo Simulation of Rarefied Flow Along a Flat Plate," AIAA Paper 87-1547, June 1987.

[3]Woronowicz, M. S., "Application of a Vectorized Particle Simulation to the Study of Plates and Wedges in High-Speed Rarefied Flow," Ph.D. Dissertation, Dept. of Aeronautics and Astronautics, Stanford Univ., Stanford, CA, June 1991.

[4]Haas, B. L., "Particle Simulation of Rarefied Aeropass Maneuvers of the Magellan Spacecraft," *Journal of Spacecraft and Rockets*, Vol. 31, No. 1, 1994, pp. 17–24 (AIAA Paper 92-2923, July 1992).

[5]Baganoff, D., and McDonald, J. D., "A Collision-Selection Rule for a Particle Simulation Method Suited to Vector Computers," *Physics of Fluids A*, Vol. 2, July 1990, pp. 1248–1259.

[6]McDonald, J. D., "A Computationally-Efficient Particle Simulation Method Suited to Vector Computer Architectures," Ph.D. Dissertation, Dept. of Aeronautics and Astronautics, Stanford Univ., Stanford, CA, Dec. 1989.

[7]Whitfield, D. L., "Mean Free Path of Emitted Molecules and Correlation of Sphere Drag Data," *AIAA Journal*, Vol. 11, No. 12, 1973, pp. 1666–1670.

[8]Bird, G. A., "Definition of Mean Free Path for Real Gases," *Physics of Fluids*, Vol. 26, Nov. 1983, pp. 3222, 3223.

[9]Woronowicz, M. S., and Baganoff, D., "Drag and Heat Transfer Correlations for Rarefied Hypersonic Flow Past Flat Plates," *Journal of Thermophysics and Heat Transfer*, Vol. 7, No. 1, 1993, pp. 63–67.

[10]Gilmore, M. R., and Harvey, J. H., "Effects of Mach Number, T_{wall}, T_∞, and Thermal Accommodation Coefficient on Flow Around Bluff Bodies in the Rarefied Regime," 18th Symposium on Rarefied Gas Dynamics, Vancouver, BC, Canada, July 1992.

[11]Oppendheim, A. K., "Generalized Theory of Convective Heat Transfer in a Free-Molecule Flow," *Journal of the Aeronautical Sciences*, Vol. 20, Jan. 1953, pp. 49–58.